RSC Advances

PAPER

View Article Online
View Journal | View Issue

Cite this: *RSC Adv.*, 2026, **16**, 16264

From pen to paper-based screening: an early-stage colorimetric μPAD with desktop-app readout for lead and nitrite

Akashlina Basu, [a] Pooja C. Asani, [a] Kalpita Nath [b] and Soumen Das *[a]

Industrial wastewater often contains several toxic contaminants, among which lead (Pb^{2+}) and nitrite (NO_2^-) ions are regarded as significant contributors to human health risks. These are readily absorbed by humans *via* drinking and agriculture. This growing public health concerns demand urgent, on-site screening as it is a crucial step for monitoring industrial effluent hotspots in both rural and urban communities. Detection of these requires the use of complicated gold standard technology such as Atomic Absorption Spectroscopy, High Performance Liquid Chromatography and so on, which is challenging to establish at testing locations and much more difficult for laypersons to comprehend. Hence, the present work seeks to create a straightforward colorimetric paper sensor for the simultaneous screening of lead and nitrite ions in aqueous solutions, which combines facile fabrication methods with easy interpretation. The sensor utilises sodium rhodizonate and Griess reagent modified paper for the colorimetric readout. The readout can be obtained using a standard smartphone camera connected to the darkroom, simulating attachment to guarantee uniform lighting conditions. Further to counter the problems of reagent decomposition, a graphite-based reagent pencil has been fabricated that increases the solid-state stability of sodium rhodizonate on paper from 2 hours to more than 2 months under light-protected storage, independent of the nitrite assay components. Additionally, to fully integrate the sensor into an accessible detection system, a lightweight machine learning regression model coupled with a graphic user interface through desktop application has been used for semi-quantitative interpretation of the smartphone images. The model achieved an *R*-squared value of 0.95 and 0.96 for lead and nitrite ions, respectively. Colorimetric responses on the paper sensor were evaluated using samples collected from various water bodies and agricultural lands. The algorithm accurately predicted concentrations, achieving detection limits of 7 ppm for lead and 3 ppm for nitrite. The sensor's performance showed minimal influence from ambient temperature and humidity. Overall, a simple paper-based semi-quantitative approach for preliminary screening of common water pollutants at sites of highly contaminated water samples influenced by industrial activities could be demonstrated as a proof of concept.

Received 9th December 2025
Accepted 11th March 2026

DOI: 10.1039/d5ra09526c

rsc.li/rsc-advances

Introduction

Lead pollution and heavy metal contamination in the environment is a global concern.[1] The rise in atmospheric lead levels is contributed majorly by human activities, including mining, fossil fuel burning, manufacturing of paints, explosives, batteries, *etc.*[2] Additionally, old pipes and solder joints, ceramics, and toys are all sources of lead contamination.[3] Lead is not directly involved in any biological processes in the human body, and, therefore, it is toxic at even very low concentrations. Plumbism or lead toxicity affects various organs in the body, and it is more detrimental for women and children. Since lead is majorly absorbed into the bloodstream, it gets carried to different organ systems and causes haemolytic anaemia due to binding with haemoglobin inside erythrocytes.[4] In adults, prolonged exposure to lead can cause kidney damage, high blood pressure, hearing problems, hyperactivity, cancer, and reproductive disorders.[5–7] Moreover, children who are continuously exposed to lead contamination show slow motor responses, decreased IQ, hypertension, and growth disorders.[8] Alarmingly, lead nitrate concentrations have been reported to exceed the recommended limits in industrial wastewater from regions such as Taiwan and the Philippines.[9] A similar trend has been noticed in wastewater discharge from paint and other industries in studies performed for industrial areas of Lagos, Swabi, and Kirkuk City.[10–12] Several studies performed across central India, West Bengal, and coastal areas indicate severe pollution of the environment by heavy metals, including lead.[13–15] The

[a]*School of Medical Science and Technology, Indian Institute of Technology, Kharagpur, West Bengal, India. E-mail: sou@smst.iitkgp.ac.in*
[b]*Department of Chemical Engineering, Indian Institute of Technology, Kharagpur, West Bengal, India*

predominant cause of this contamination is the burning of coal and other industrial processes.

Another pollutant found in industrial wastewater, nitrite, is a vital nutrient ion involved in the growth and development of plants. Nitrite is derived from reduction of nitrates which is major component of most fertilizers. However, increasing industrialization and urbanization have adversely affected the balance of the nitrogen compounds in the environment. Additionally, a substantial amount of nitrite is utilized in applications in the industrial and healthcare sectors.[16–18] Therefore, nitrite pollution has become a global concern that is ubiquitously present in food, water, soil, environment, and even physiological systems. Presence of nitrite in water bodies has been seen to increase the acidity of water due to generation of nitrous acid. This acidity further interacts with insoluble lead in wastewater, increasing the risk of heavy metal poisoning by ingestion of soluble lead.[19,20] In humans, nitrite interacts with proteins to form *N*-nitrosamines, leading to severe outcomes like gastric and oesophageal cancer, blue infant syndrome, spontaneous abortion, and birth defects in the Central nervous system.[21–23] Nitrite can be present as particulate matter in ambient air, causing asthma and severe incidences of impaired lung functions.[24] In India, several case studies have been performed in Odisha, Gujarat, Uttar Pradesh, and other states which indicate extensive nitrite pollution in the environment aided by various human activities, including, overuse of fertilizers, burning crackers during festivals, improper waste disposal, *etc.*[25–27] The Central Pollution Control Board in India has stated that the maximum allowed limit for nitrite compounds in industrial effluents is 50 mg l^{-1} (ppm) and for lead, it lies between 0.1 to 10 mg l^{-1} (ppm) for various industries.[28] Reports released by the Pure Earth organization and CSIR-NITI Aayog organisations in India have revealed that the BLL (blood lead levels) in Indian children is much above the average safe limits, purportedly due to violation of the effluent treatment plans set by the government.[29,30] This situation warrants regular screening of lead and nitrite ion levels in the environment, especially.

The existing methods for monitoring lead include UV-visible spectrometry (UV-vis), Atomic Absorption Spectroscopy (AAS), Mass spectroscopy (MS), X-ray Fluorescence (XRF), and Cyclic Voltammetry.[31–35] Similarly, current methods of nitrite detection include chromatography, spectrophotometry, surface enhanced Raman spectroscopy, capillary electrophoresis, fluorescence spectroscopy, chemiluminescence, and electrochemical methods.[36–42] Even though these techniques are widely accepted, they are accompanied by several limitations like high cost of equipment, requirement for trained personnel, bulky nature of the instrument, need for sample processing/pretreatment, and long analysis times.[43,44] While ppb level sensitivity is crucial for regulatory drinking water analysis, polluted sample analysis requires rapid triage tools that offer moderate sensitivity with high efficacy, instead of attempting a highly sensitive but costly analysis procedure in a laboratory. Hence, there is a requirement for a cost-effective, user-friendly, and field-deployable detection technique in resource-limited regions for these ions in the environment. Raw effluents from battery manufacturing, mining, and electroplating industries require pre-treatment screening to ensure effective contaminant removal, making these settings ideal for the application of a semi-quantitative paper-based sensor.

In this direction, Paper micro-PADs (μPads) were introduced in 2007 by the Whitesides group as a viable alternative enabling the development of rapid, reliable and field deployable monitoring systems.[45,46] As reported by O. Kare *et al.*, paper devices can be incinerated to very little residue within 20 seconds, which allows for environment-friendly development of sensors.[47] Paper-based devices utilize capillary action to transport fluids through paper, eliminating the need for an external pump.[48–50] These devices follow the REASSURED (Real Time Connectivity, Ease of specimen collection, Affordable, Sensitive, Specific, User friendly, Rapid and Robust, Equipment free and Deliverable) criteria set by WHO for bringing the laboratory to a chip for remote location needs.[51] These devices work by creating hydrophobic boundaries on paper using polymers that can penetrate through pores to design sample wells or channels as per the requirements of the test.[52] In the past, wax printing was used mainly for drawing hydrophobic channels on paper. However, due to the recent discontinuation of wax printers, other methods are being chosen. Those include the use of polydimethylsiloxane (PDMS), polystyrene, and other resins. Research has also been done on using ink-jet printing and protein aggregation as mechanisms to form hydrophobic boundaries that require heat treatments. In this research, permanent ink markers were used to create hydrophobic wells on paper due to ease of application, as reported by several researchers working on pen and paper sensing devices.[53,54]

Recently, μPads associated with colorimetric reactions have gained much attention for the detection of heavy metals, along with organic, and inorganic species.[55] Colorimetric assays are preferred for their simplicity, low cost, ease of use by inexperienced individuals, rapid on-site detection, multiplexed, and straightforward interpretation of results by the naked eye.[13] These devices also provide improved sensitivity, detection limits, and a user-friendly interface.[56] Scanners, digital cameras, and smartphones, along with imaging software like ImageJ and Adobe Photoshop, can be employed as quick, and easy ways to assess the colour intensity of μPADs to get a quantitative readout.[44,57]

An issue often encountered in reagent modified sensors, is the decomposition of these reagents due to effects of light, heat or humidity. To address the limitations of solution-based deposited reagents on paper devices, reagent pencils were first fabricated by Mitchell *et al.*[58] They used a mixture of polyethylene glycol methyl ethyl and graphite as binders for the reagent. Subsequently, Liu *et al.* further characterised this fabrication method to optimise the reagent concentration being loaded onto the paper.[59] In the current study, a reagent pencil was designed to counter the problem of rapid decomposition of sodium rhodizonate in solution. Bentonite clay was used as the binder for the powder, while the graphite was used to form a matrix structure to trap reagent particles and facilitate deposition on paper. Since this powder mixture does not involve water as a binder, it is hypothesized that the reagent stability should be enhanced.

This work presents a field-deployable, cost-effective, and user-friendly colorimetric sensor based on pen and paper microfluidics for the preliminary screening of lead and nitrite at the sites where industrial wastewater pollution occurs. The sensor is fabricated using commonly accessible Grade 1 filter paper and permanent markers to create the hydrophobic barrier. The reagents are applied to the paper device using the conventional drop-casting technique and a unique reagent pencil deposition method, which safeguards the easily degradable chemicals from environmental conditions, allowing the device to be stored for several days and transported for field testing without compromising the colorimetric reaction. There is a lack of published research investigating the use of sodium rhodizonate in pellet form for prolonging shelf-life, which is a key factor in the current study. The colorimetric product is captured using a regular smartphone camera and a custom darkroom setup that eliminates the effects of ambient light conditions on image intensity. The analysis of the resulting image is executed using a Python-based Machine Learning approach and a desktop program to enhance automation, as detailed in this study. The production of these sensors requires minimal technical expertise, facilitating development in any distant area.

Colorimetric reaction pathways for Pb^{2+} and NO_2^-

The reagent used in this study for sensing of lead ions is sodium rhodizonate. This assay is used frequently in the field of forensic science for the detection of lead in gunshot residue. Rhodizonate is a six-member ringed aromatic oxo-carbon compound that is highly stable in solid form. It is available as a greenish powder that gives an orangish-yellow solution when dissolved in distilled water as it forms rhodizonic acid. This solution is highly unstable and decomposes rapidly, even when refrigerated. Lead forms coordinate bonds with the oxygen pair present in rhodizonic acid that results in the formation of pink rod-shaped lead rhodizonate complex crystals (Fig. 1(a)). The intensity of this reddish pink colour depends on the concentration of lead ions in the solution.

For detection of nitrite in this study, the paper has been modified with Griess reagent. For sensing nitrate, the analyte has to be first reduced to nitrite using reducing agents such as zinc microparticles or enzymatically. Under acidic conditions, nitrite ion turns into nitrous acid that is very reactive and decomposes into nitrosonium ion (NO^+). The amine group in sulfanilic acid reacts with this nitrosonium ion to form a diazotised cation which subsequently reacts with α-naphthyl amine and undergoes azo coupling to result in a pinkish purple diazo dye (Fig. 1(b)). The intensity of this azo dye product assists in the determination of the nitrite content in a sample.

Methodology

Chemicals and instrumentation

Lead nitrate, calcium chloride, magnesium oxide, potassium chloride, ferric chloride, chitosan powder, sodium chloride, sodium nitrite, barium chloride, sulphanilic acid, trehalose dihydrate, orthophosphoric acid, *N*-(1-naphthyl) ethylenediamine dihydrochloride (NED) and sodium rhodizonate was purchased laboratory grade from Sisco Research Laboratories Pvt. Ltd Whatman Filter Paper Grade No-1 Size 110 mm diameter was obtained from Sigma-Aldrich. Permanent marker pens were acquired of the Camlin brand from local shops. De-ionized water (DI water) is used to prepare all aqueous solutions used in this work (resistivity of 18.2 MΩ cm at 25 °C).

SHIMADZU UV VIS Spectrophotometer (UV 1800) was used to understand the reactions between the reagents and the analytes with varying concentrations. Cuvettes with 1 cm path length and 3 ml capacity were used for this purpose. Atomic Absorption Spectroscopy (PerkinElmer, USA) was used as the gold standard method for analysis of real and spiked lead ion samples. For optical microscopic observations, Nikon Eclipse Ts2R inverted microscope was used. FESEM, Merlin, ZEISS Corp., Germany was used for scanning electron microscopy images.

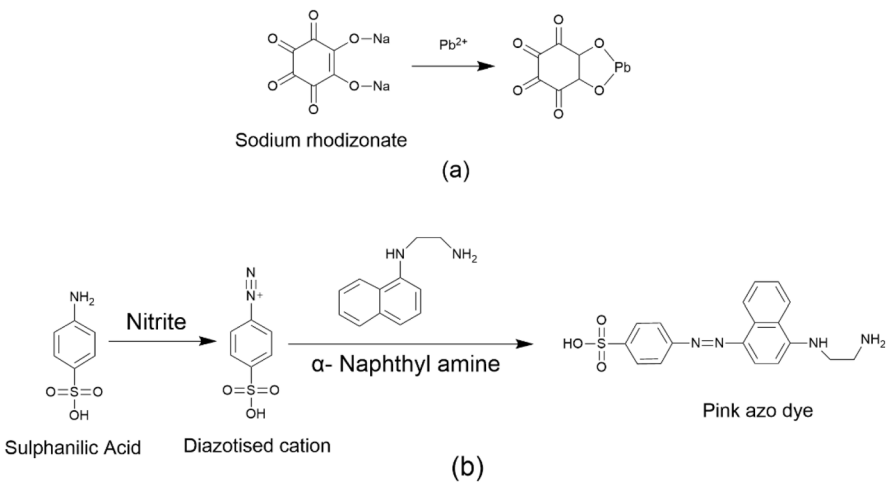

Fig. 1 Reaction mechanism (a) between lead ions and sodium rhodizonate reagent. (b) Development of azo dye due to interaction between nitrite and Griess reagent.

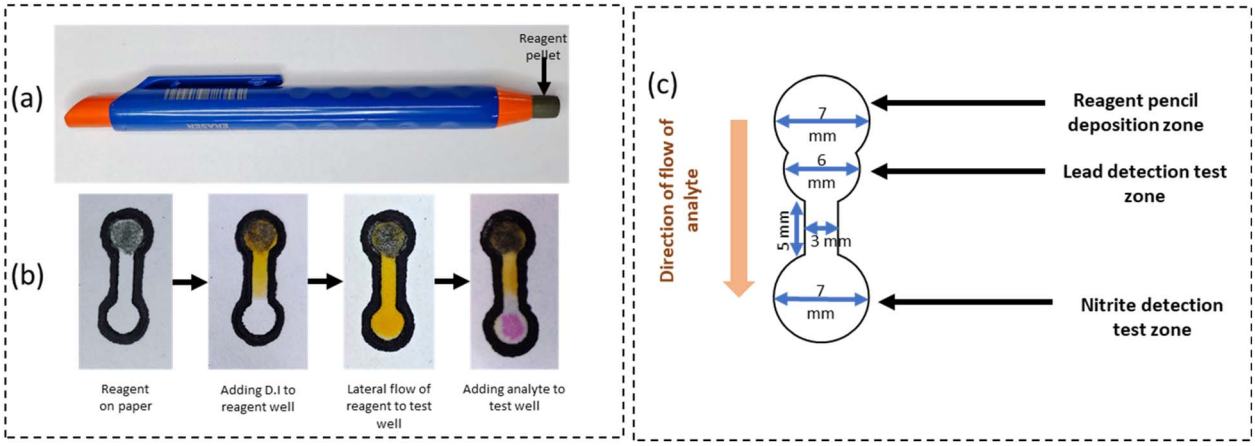

Fig. 2 (a) Mechanical eraser holder with the loaded reagent pencil with (b) a flowchart demonstrating the method of utilising the developed pellet for lead detection (not the final device design). (c) Dimensional representation of the final design of the colorimetric sensor.

Fabrication of reagent pencil

The reagent pellet used in this study was made from a powder mixture consisting 6 grams of bentonite clay, 2 grams of graphite powder, and 1.2 grams of sodium rhodizonate reagent powder. This combination was subjected to high pressure (~8–10 ton) in a hydraulic pellet press with a 5 mm internal diameter mould. The pellet was then carefully preserved in a soft cotton cloth at 4 °C to avoid contact with ambient moisture. During the trials, the pellet was inserted into a mechanical eraser holder, as shown in Fig. 2(a), and rubbed against the reagent deposition zone of the paper device. The reagent pencil strokes were applied so that the same weight of powder blend, *i.e.* 0.5 milligrams was deposited on the deposition zone for each device. When de-ionised (DI) water is added in microliter quantities to the deposition zone, the reagent powder reacts with it, creating rhodizonic acid that flows along the defined channel *via* the paper's capillary action. As it enters the test zone, analyte can be introduced to initiate the colorimetric response. This process of converting the reagent from a solid pellet to a reagent solution and using paper capillary action to guide it towards the analyte zone is demonstrated in a flowchart in Fig. 2(b). Along with reagent pencil, Griess reagent was prepared by mixing a 1 : 1 ratio of 1% sulfanilic acid solution in 5% ortho-phosphoric acid and 0.1% NED solution in DI 2% trehalose solution was added to the reagent to increase shelf-life. Chitosan solution was prepared using 0.5% chitosan in 2% acetic acid.

Paper device fabrication

The keyhole-shaped design of the sensor was designed in freeware software, Inkscape. The design of the sensor includes two attached circular wells of 7 mm and 6 mm diameter connected to another circle of 7 mm diameter by a passage of 3 × 5 mm dimensions (Fig. 2(c)). The designs were laser-printed on the filter paper of Grade 1 and were overlined with permanent marker ink pens to form hydrophobic boundaries. The reagent pellet was used on the deposition zone to deposit sodium rhodizonate. Further, 3 μl of Griess reagent was drop-casted on the nitrite detection zone. Then the paper devices were stored in dark containers and air tight conditions before further experimentation.

Experimental procedure

To develop a training data set for colorimetric assay, solutions of lead and nitrite in concentrations, varying from 1 to 100 ppm was prepared through serial dilutions in DI water. The solutions were first pre-processed with acetic acid using capillary tubes of 5 μl volume twice, so that the final volume of acid added was 10 μl. The acetic acid is added to the sample to ensure that the lead rhodizonate crystals formed do not aggregate between the paper's pores and allow the colours to spread farther. This phenomenon is elaborated later in this manuscript.

The sodium rhodizonate in the deposition zone was activated using DI water to allow lateral spread of reagent into the test zone for lead and allowed to dry. After 5 minutes, 6.5 μl analyte solution was added to the lead detection zone. The solution is allowed to flow from the lead detection zone to the nitrite detection zone. A custom darkroom arrangement was designed in AutoCAD and 3D printed to capture images of coloured output on the paper sensor, which is referred to as 'dark box' in this study. The distance between the camera and the paper device was fixed at 8 cm when designing the custom dark box. Each paper device was attached to the sample holder in the dark box using double sided tapes and photographs were captured using smartphone camera (Make: Motorola Edge 50 Fusion, 50 MP rear camera). Exposure compensation was manually locked at −3.0 eV to prevent automatic brightness adjustment. Autofocus was turned off and white balance were kept constant during image acquisition. All images were captured exactly 5 minutes after sample placement using identical camera settings for all measurements. The procedure followed for the development of coloured product on the paper sensor is given in Fig. 3(a). Fig. 3(b) depicts the dark box setup which was built as a smartphone attachment to provide portability and consistent lighting settings for all images, independent of ambient conditions. The portable darkroom environment simulating box featured a centre chamber with a smartphone positioned above it. A hole is carved into the roof of this dark box based on the curves of the smartphone's camera positioning. Four LEDs are positioned beneath this ceiling to

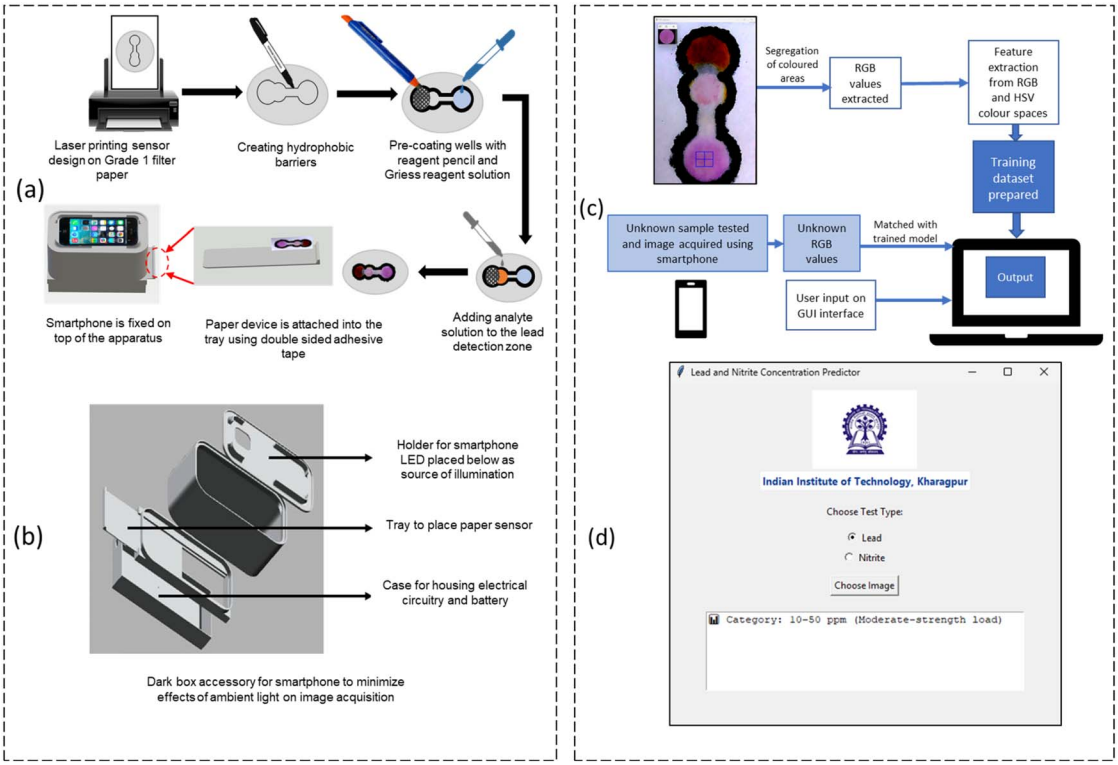

Fig. 3 (a) demonstrates procedure followed for the development of coloured product on the paper sensor while (b) depicts the arrangement of the dark room apparatus. (c) Flowchart of the python-based regression method adopted for the analysis of colorimetric images on paper. (d) GUI interface for user-friendly prediction of analyte concentration.

provide even light distribution. Underneath this chamber is a tray on which the paper sensor can be attached using adhesives for photography purposes. The dark box's bottom section has a compartment for the electrical components that control the inside illumination. The container is completely sealed, with matte black inside surfaces that resemble the conditions seen in a traditional darkroom for photography.

Regression study and python-based framework implementation

A Python-based image processing algorithm was developed to analyze colorimetric sensor images and generate user-readable results. For the training dataset, cropped images containing only the coloured reaction areas were compiled. This dataset was processed by a Python script that extracted RGB and HSV values from each image using the NumPy and OpenCV libraries and saved the data in a CSV file. This file then served to train a regression model, which was saved as a Pickle file to streamline future predictions by avoiding retraining. For optimization experiments, mean grey intensity was calculated from the mean R, G and B values using OpenCV's greyscale conversion command that utilises the following formula.

$$\text{Mean grey intensity} = 0.299 \times R + 0.587 \times G + 0.114 \times B$$

A Support Vector Regressor model with a radial basis function (RBF) kernel was used to test the efficiency of concentration prediction. The hyperparameters were set as $C = 100$, $\varepsilon = 0.01$, and $\gamma =$ 'scale', where γ is automatically determined based on feature variance to balance flexibility and generalisation amid image variability commonly seen in smartphone images captured of paper-based devices. The Python script used for this purpose makes use of the Pandas package to read tabular data. It also used the NumPy library to conduct mathematical operations on array-structured data. The data is organised into seven columns: red intensity, green intensity, blue intensity, hue, saturation, intensity and concentration (in ppm). The first six columns are then retrieved for input and assigned to the variable 'x', while the final column is assigned to the variable 'y'. Here, x is the dependent variable and y is the independent variable. The data was then separated into training and testing datasets at an 80 : 20 ratio. To avoid data leakage, all preprocessing and regression steps were implemented within a scikit-learn pipeline, ensuring that feature scaling parameters were learned exclusively from the training data. The dataset was randomly divided into training (80%) and testing (20%) subsets at the sample level using a fixed random seed. Model robustness was further evaluated using 5-fold cross-validation.

During prediction, the user selects a rectangular region of interest (ROI) *via* OpenCV's selectROI function, followed by defining a circular mask within this ROI using cv2.circle. A binary mask isolates the colorimetric reaction area by setting all pixels outside the circle to black (0) and inside to white (255). The bitwise operation retains pixel values only within the reaction zone, allowing extraction of mean RGB values. These

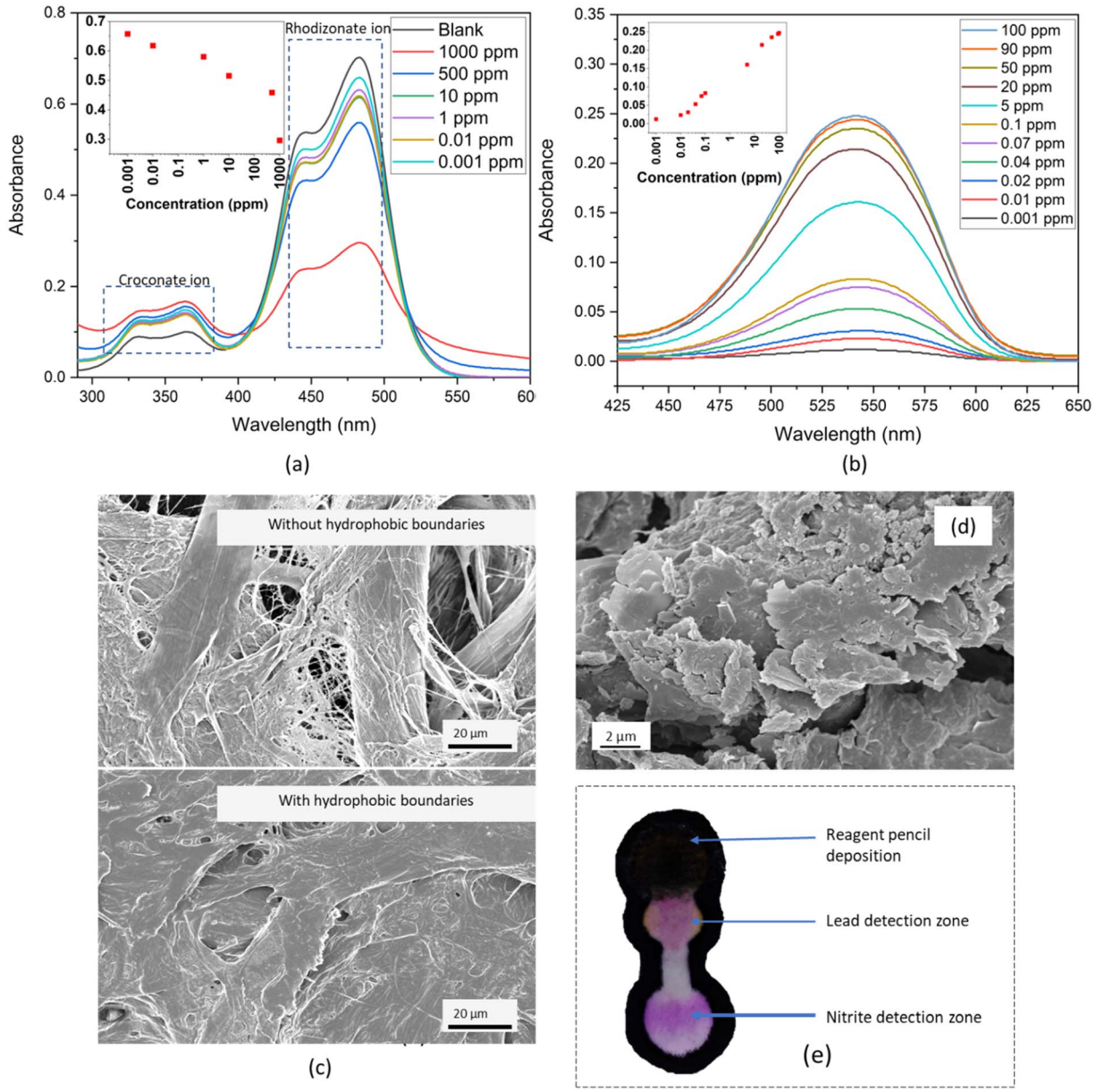

Fig. 4 UV visible peaks for (a) reaction between lead and sodium rhodizonate reagent; (b) reaction between nitrite and Griess reagent. SEM images of (c) bare paper and paper with hydrophobic boundary, (d) paper with sodium rhodizonate pellet deposition. (e) Final image of the sensor demonstrating the coloured product developed due to positive test for presence of lead and nitrite.

RGB values are then input into the trained regression model to predict the analyte concentration. This workflow is summarized in the flowchart shown in Fig. 3(c), with pseudocode provided in Table S1 of the SI. To enhance usability, a graphical user interface (GUI) was created using the Tkinter module, as shown in Fig. 3(d). Users choose whether to analyze lead or nitrite, upload the corresponding image, and select the ROI. The regression model with optimal results is loaded, and the final output displays the analyte concentration in terms of three categories, which were low strength (<10 ppm), moderate strength (10–50 ppm) and high strength (>50 ppm) loads of contamination.

Results and discussions

UV-visible spectroscopy analysis for Pb^{2+} and NO_2^- detection

The UV visible absorption peak of the reaction between lead ions and sodium rhodizonate shows two peaks, one at ~486 nm with a shoulder peak at ~440 nm which corresponds to the rhodizonate ion, while another peak can be seen at ~365 nm with a shoulder peak at ~325 nm that corresponds to the UV visible peak for croconate ion (Fig. 4(a)). The inset graph represents the reduction in peak absorbance of the rhodizonate ion with concentration. It can be noticed that when blank sample is run under UV spectrometer, the intensity of the rhodizonate peak is much higher than that of the croconate

peak, indicating the photocatalysis of rhodizonate ions and conversion to croconate ions. Further, a trend of decrease in rhodizonate peaks with a corresponding increase in the croconate peak can be noticed with the increasing concentration of lead in sample. It can be hypothesized that the conversion of sodium rhodizonate to lead rhodizonate increases the photochemical activity in the reagent solution. The decrease in peak intensity of rhodizonate ion can be seen for concentration as low as 1 ppb of lead.

The UV visible absorption peak for the azo dye that forms on reaction between nitrite and Griess reagent can be noticed at 545 nm, as shown in Fig. 4(b) with the peak absorbance intensities plotted in inset graph. It is seen that with an increase in concentration of nitrite the peak seen at 545 nm increases as well. The peak could be mapped for a minimum concentration of 10 ppb nitrite, proving this reagent extremely sensitive for detection in aqueous media.

Optimisation of experimental parameters

Design, volume, and time optimisation. Hydrophobic barriers were necessary to be formed on paper to direct the flow of the analyte solution and confine the reagent solutions. Various techniques for hydrophobic boundary construction have been investigated in literature, including laser jet printing, wax printing, and BSA protein agglutination. In the present study, marker pen ink was identified as the most suitable option because of its cost-effectiveness and lack of required processing techniques, such as heating. Furthermore, the borders defined with marker pen ink are unaffected by the low pH environments necessary for conducting the current experiments (Fig. S1). Observation of paper under a Scanning Electron Microscope (SEM), both with and without marker pen ink deposition (Fig. 4(c)), revealed that the paper fibres were entirely encased in the resin from the marker pen ink, rendering them impervious to fluids.

The sensor was designed in such a way that the analyte solution first reacted with the lead detection reagent and then flowed to the detection zone for nitrite. This allowed for the formation of lead rhodizonate crystals first and then the azo dye formation with nitrite. It was observed experimentally that if the analyte was not added exactly on top of the lead detection reagent area, it did not form sufficiently quantifiable coloured crystals for further analysis. The accurate measurement of the volume to be added to the reaction well is another critical factor for analysis. Insufficient reagent or analyte solution addition to the well results in non-uniform distribution within the reaction zone, leading to inaccurate colour development. If the volume of analyte solutions surpasses the optimised volume, a droplet forms on the paper, potentially spilling over the hydrophobic boundary. Additionally, the presence of liquid atop the cellulose fibres leads to light reflection during image capture, resulting in inaccurate colour measurements.

When the reagent pencil was applied to the deposition zones of the paper device, a weight of 0.5 ± 0.03 g was maintained for all the devices. Fig. 4(d) illustrates the SEM image of the deposited reagent pellet, which thoroughly coats the paper fibres. The activation of the sodium rhodizonate reagent in this deposition required 5 μl of deionised water, which effectively mixed with the reagent pencil deposition on paper, generating sufficient reagent to adequately fill the lead detection test zone without excessive diffusion into the connecting passage. Likewise, 3 μl of Griess reagent completely occupied the nitrite detection zone without interfering with the sodium rhodizonate reagent. To prevent the flow of Griess reagent further into the connecting path between the wells, a layer of chitosan was first added to the nitrite detection well. Chitosan acts as a physical binder for the multiple layers of Griess reagent, while also preventing coffee ring formation when the azo dye develops. Given that the paper device was designed to facilitate the passage of the analyte solution from the lead detection zone to the nitrite detection zone, as seen in Fig. 4(e), volume optimisation was essential. When quantities less than 6.5 μl were introduced and evaporated for 5 minutes, the solution failed to exhibit enough reactivity with sodium rhodizonate and did not reach the nitrite detection test zone. If the volume surpassed 7 μl, the sample over-flowed from the nitrite detection area, resulting in inadequate azo dye production for imaging and quantification. The optimal volume of analyte solution for the lead detection zone in the selected sensor design was fixed to be 6.5 μl.

A further critical element of optimisation was identified as the period of time required for colour development prior to image capture. Initially, the analyte solution requires around 4–5 minutes to properly spread in the lead detection zone, interact with the reagent and then travel to the nitrite detection zone using capillary action. Therefore, the image capture was started only after 5 minutes of adding analyte. The coloured product formed on paper attained maximum brightness within a few minutes of the reaction, after which its colour intensity diminished. A more vibrant colour on paper correlates with a deeper grey value, as the values approach 0 (the value for absolute black), whereas a less intense colour corresponds to lighter grey values, as the colour values approach 255 (the value for absolute white). Fig. 5(a and b) illustrates that for both the lead and nitrite detection assays, the maximum visible pink hue occurred at 5 minutes post-reaction, subsequently diminishing to a muted pink. Therefore, all image captures were conducted precisely five minutes post-reaction.

Influence of acid, temperature and humidity. The role of acetic acid in forming a coloured complex between sodium rhodizonate and lead was also investigated. It was discovered that the complex formed in the absence of acetic acid was reddish-purple in colour and did not spread far from the analyte deposition site. The same trend was seen in colorimetric reactions for bismuth and copper in water samples on paper.[60] The reaction of sodium rhodizonate with lead in the absence of acid produced rod-shaped crystals with an average size of 22 μm, as shown in Fig. 5(c(i)). Because this exceeds the pore size of filter paper Grade 1, the pores become clogged, resulting in less spread of the coloured complex as seen in Fig. 5(c(iii)). Addition of acetic acid breaks these crystals into smaller sizes (Fig. 5(c(ii))), which directly results in a diffused area of colour development in the test zone, as seen in Fig. 5(c(iv)). Fig. 5(d)

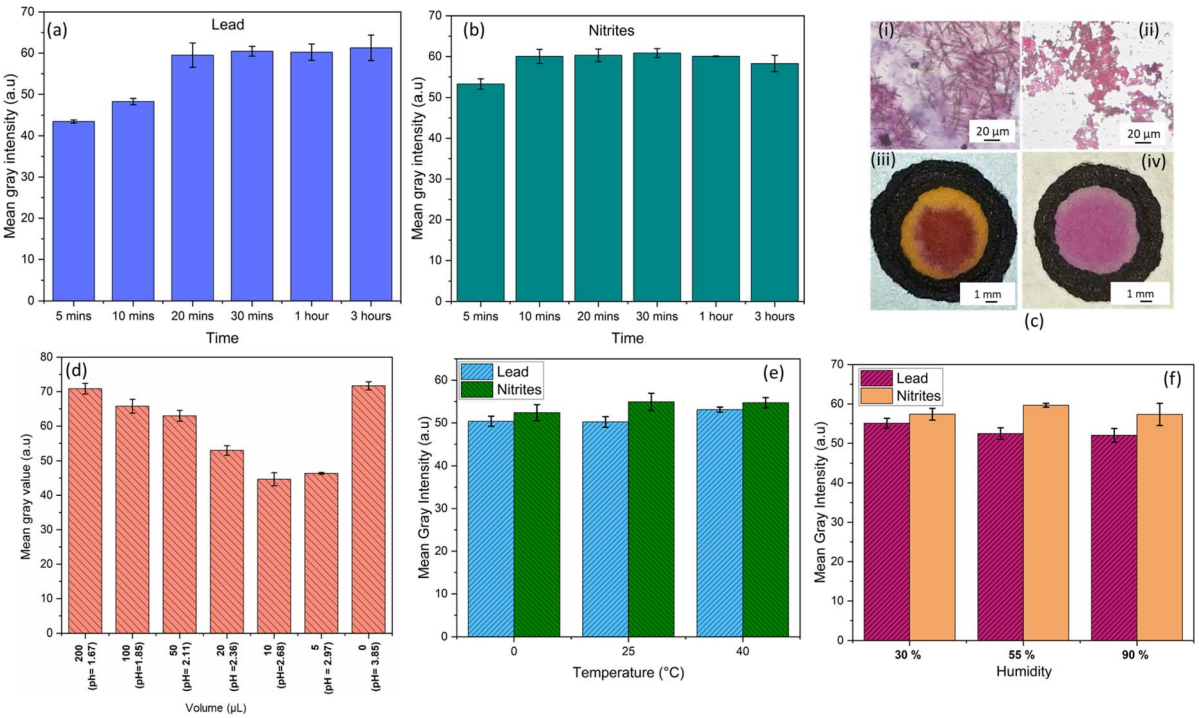

Fig. 5 Comparison of the effects of time, pH, temperature and humidity on the colour development in multiplexed sensor. (a) and (b) represent the changes in colour development of the sensor for lead and nitrite respectively, for optimisation of the time of image capture. (c) Effects of acetic acid on the reaction between sodium rhodizonate and lead. (i) and (iii) depict the coloured products of the reaction in absence of acetic acid, and (ii) and (iv) depict the coloured products formed in presence of acetic acid. (d) Comparison of mean grey colour intensities for various volumes of acetic acid with their corresponding pH values. (e) Comparison plots for the mean grey intensities for assays of lead and nitrite at different temperature points. (f) Comparison plots for the mean grey intensities for assays of lead and nitrite at different humidity conditions.

demonstrates effect of pH on the lead rhodizonate crystal formation by adding various volumes of acetic acid to 1 ml equimolar solutions of lead for examination of the best conditions for coloured product development on paper. With high volumes of acetic acid, it was seen that the intensity of the pink colour developed was lower resulting in higher grey intensity values. It can be hypothesized that higher acidity breaks the crystals of lead rhodizonate into smaller sizes due to which they diffuse further away in the pores of paper resulting in unquantifiable colour development. It was concluded experimentally that a volume of 10 µl of acetic acid which corresponds to a pH value of 2.68, could give the brightest pink-coloured product on paper. Furthermore, the acidification of the analyte solution also helped with the conversion of nitrite to nitrous acid, making it even more reactive. Therefore, all the experiments were performed with analytes treated with 10 µl of acetic acid per 1 ml of sample.

The sensor was evaluated under diverse temperature and humidity circumstances to guarantee its robust functionality in variable weather environments, using equimolar concentrations of lead and nitrite. Three temperature settings were simulated to mimic severe heat, extreme cold, and ambient temperatures at 0, 25, and 40 °C, respectively. The average grey values exhibited minimal variation for both lead and nitrite assays. It was observed that at further elevated temperatures, the colour development was slightly less intense, resulting in slightly higher grey values, as illustrated in Fig. 5(e). The rationale for this phenomenon is that elevated temperatures accelerate the evaporation of the analyte solution on paper, leading to a brief liquid–liquid interaction between the analyte and reagent, which leads to diminished colour intensity development. The three humidity levels examined were 30%, 55%, and 99% and their corresponding grey value intensities are compared in Fig. 5(f). The colour intensities for lead and nitrite testing were consistent across all humidity conditions, exhibiting minimal error. It may be concluded that the devices function effectively in most temperature and humidity settings; however, tests should be conducted away from sunlight to mitigate the effects of evaporation.

Stability and selectivity of reagents on paper. Selectivity study was conducted to evaluate the response of the paper-based sensor towards target analytes in presence of commonly present interfering species. Nitrite and lead solutions were prepared at a concentration of 40 ppm. Commonly present ions such as Mg^{2+}, Ca^{2+}, Cl^{-} *etc.* were tested at a higher concentration (200 ppm), while less commonly encountered ions such as Fe^{3+}, Hg^{2+}, and Ba^{2+} were tested at 40 ppm, matching the analyte concentration. Each analyte was evaluated individually in the presence of each interferent and in a mixed matrix condition involving all ions together. Subsequently, colorimetric response was quantified using the inverted green channel intensity ($255 - G$), where G represents the green channel value

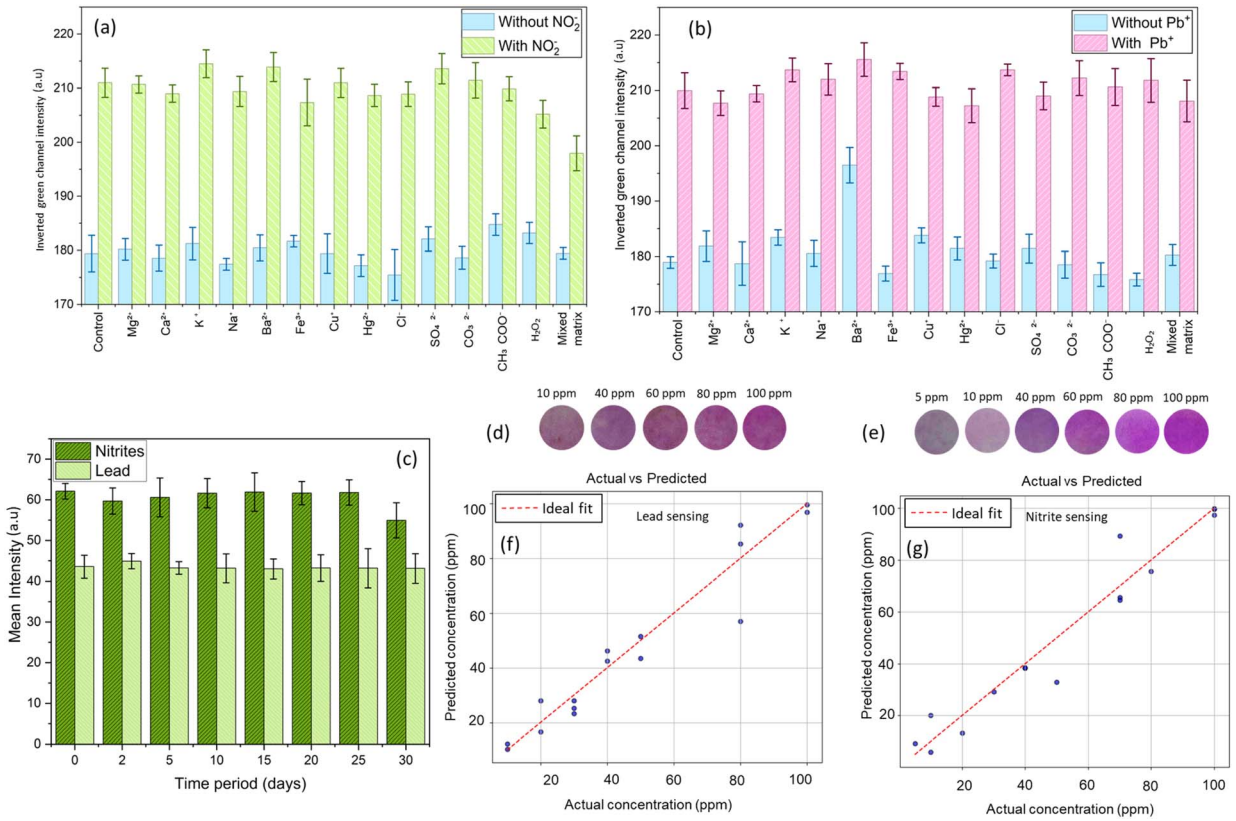

Fig. 6 Selectivity of reagent pencil for (a) nitrite and (b) lead compared with commonly available metal ion interferants in polluted waters. (c) Stability tests for a period of 30 days for sodium rhodizonate in reagent pencil form and Griess reagent solution in presence of 100 ppm salt solution containing lead and nitrite ions. Comparison of the different colour intensities developed due to presence of (d) lead ions and (e) nitrite ions in salt of various concentrations on reagent infused paper sensor. Actual *vs.* predicted plot for SVR model predicting concentration of (f) lead and (g) nitrite.

in the RGB colour space, such that increasing values correspond to stronger development of the characteristic pink chromophore. Fig. 6(a and b) illustrates colour intensity differences for reaction in the absence and presence of our target ions. The selectivity of the Griess reagent in presence of nitrite, has been previously reported in the literature which indicates that Fe^{3+} ion seems to lower the azo dye intensity but all other ions prevalent in industrial discharge show negligible interference.[61] The presence of oxidizing species (H_2O_2) and Fe^{3+} ions resulted in a noticeable reduction in colour intensity in our study as well. This effect is consistent with the known susceptibility of the Griess reaction to oxidation and metal-ion interference, as given in literature. In contrast, commonly occurring background ions showed negligible influence on the nitrite response at the tested concentrations. To mitigate the problems faced due to presence of oxidising species and Fe^{3+} ion, literature suggests pre-treatment steps involving masking agents such as EDTA (ethylenediaminetetraacetic acid)[62] and enzymes like catalase which support oxidant scavenging behaviour.[63] In wastewater environments, the presence of nitrates along with reducing agents could lead to partial reduction of nitrates to nitrites, which can slightly influence the Griess response. This is a known limitation of nitrite-based colorimetric detection and should be considered when interpreting results in complex industrial effluents. Further, literature also reported that Griess reagent seems to work better on paper at lower pH due to the enhanced presence of nitrous acid. The incorporation of acetic acid therefore, facilitates the process indirectly. In case of lead detection using sodium rhodizonate, Ba^{2+} produced a distinct orange colouration, in agreement with previously reported interactions of rhodizonate with alkaline earth metals. However, the intensity of this response was substantially lower than that of the pink complex formed with Pb^{2+}. Consequently, in mixed-matrix experiments, the presence of Ba^{2+} did not significantly interfere with the lead-dependent colour response, and the characteristic pink colouration associated with Pb^{2+} remained clearly distinguishable. In conclusion, these results demonstrate that the proposed paper-based sensor exhibits adequate selectivity for both nitrite and lead under conditions relevant to industrial wastewater screening.

The stability of the reagents on paper was an important parameter for assessment of the shelf-life of these devices. To test the same, paper devices were fabricated with the hydrophobic boundaries. Then, Griess reagent with 2% trehalose was added to the test well for nitrite while the sodium rhodizonate reagent pencil was rubbed on the lead detection side of the device. After the Griess reagent solution dried in room temperature, the devices were packed inside zip-lock bags and

then covered with aluminium foils before being stored in 4 °C. The devices were tested for 30 days with a solution containing 100 ppm of lead and 100 ppm of nitrite and the mean green colour intensity was plotted in Fig. 6(c).

The stability of individual assay components and the complete paper-based device were evaluated separately. The trend showed very less change in the colour intensity for sodium rhodizonate complex with lead over the tested period. Since the rhodizonate reagent tends to stay stable in solid form, there was no change in the reagent quality after applying on paper for more than two months in light-protected storage. Meanwhile, the Griess reagent shows good chemical stability for 25 days and then a decline in stability after 25 days. The reason behind this was the slow degradation of the chemical components, especially *N*-(1-naphthyl) ethylenediamine, in Griess reagent on hydrolysis and oxidation as they interact with the functional groups present on cellulose. Addition of trehalose sugar helps prevent the degradation of this chemical component when kept in storage for at least 4 weeks. As the overall shelf life of the multiplex paper device is governed by the least stable component, the practical storage stability of the complete device is therefore estimated to be approximately 25 days, as shown in Fig. 6(c).

Performance of the regressor algorithm

Different concentrations of lead and nitrite ions were prepared to determine the linearity of the colorimetric responses, ranging from 1 to 100 ppm, with 80 readings in this range of concentration. The corresponding colour developed due to this concentration range is shown in Fig. 6(d and e). A factor to remember is that since the solutions were in salt form, the solution consisted of lead concentration of 62.5 ppm and nitrite concentration of 66.67 ppm in 100 ppm salt solution. The range of 1–100 ppm of lead and nitrite was chosen because the colour developed below 1 ppm concentrations was very difficult to quantify using a simple smartphone camera, since the coloured crystals or dye products was not able to show adequate contrast with the white background of paper. Ultimately, the colorimetric sensing could detect the presence of lead at 7 ppm while nitrite ions could be detected up to 3 ppm concentrations effectively on paper.

The traditional RGB analysis of image-based data assumes that the trends in features of the image are predominantly linear. The attempted linear regression for the colorimetric data in this study using saturation values from the HSI colour space has been presented in Fig. S3 of the SI. From the linear regression, the limit of detection (LOD $= 3\sigma/S$, where σ is the intercept error and S stands for slope of the calibration curve) could be statistically calculated to be 3.6 ppm for nitrites and 8.9 ppm for lead ions with a high uncertainty at lower concentration due to high standard deviation. However, the data generated for this study revealed a non-linear and saturating trend with increasing concentration. This is an expected behaviour in paper-based colorimetric assays due to the reagent saturation on the paper substrate and the limited dynamic range of the camera in resolving differences in colour between high concentrations. To ensure the best prediction of analyte concentrations, several Python-based regression models were considered, including standard linear regression, ridge regression, Support Vector Regression (SVR), and Random Forest regression models. A comparison of the regression performance of these four models is given in Table S3. Among the models, SVR performed the best with an *R*-squared of 0.95 and 0.96 for lead and nitrite, respectively, which is represented in Table 1. Further, the Root Mean Squared Error (RMSE) was also the lowest for SVR at 6.36 and 6.73, respectively. While the error is high for absolute quantification, it can be used to categorise the samples into low strength, moderate strength and high strength contamination loads. SVR is well-known for handling non-linear data with high accuracy that is expected in real-world scenarios. Support Vector Regression (SVR) was selected for signal interpretation due to its ability to model non-linear relationships while maintaining robust performance with limited training data. In contrast to linear and ridge regression models, which assume a strictly linear response, SVR effectively captures the non-linear and saturating behaviour observed in paper-based colorimetric signals. Compared to more complex models such as random forest regression, SVR provides improved stability and reduced risk of overfitting in small datasets, while retaining a continuous regression output. Additionally, the ε-insensitive loss function of SVR offers tolerance to minor signal variations arising from paper heterogeneity and manual reagent deposition, making it well suited for the present screening-oriented application. The model performance was evaluated by 5-fold cross-validation on the full dataset by separating the data into different training and testing sets in 80 : 20 ratio for 5 times. This resulted in a cross-validation mean R^2 of 0.87 and 0.945 for lead and nitrite, respectively. A reasoning behind this is that the use of a manually fabricated reagent pencil introduces unavoidable variability in reagent thickness and local deposition during the scribbling process. Such variability is inherent to early-stage, hand-fabricated paper-based devices and is being reflected in the model performance under cross-validation. In future iterations, automation of reagent deposition or the use of stencil- or mask-assisted writing approaches could improve uniformity and further enhance reproducibility. The observed RMSE for lead and nitrite was calculated to be 6.36 ppm and 6.73 ppm, respectively, which is mentioned in Table 1. Considering this level of prediction error near the decision threshold, the outputs were interpreted as approximate values, and the device can therefore be positioned for semi-quantitative screening rather than precise quantification. It was also observed that a high number of features resulted in poor cross-validation

Table 1 Evaluation parameters of the algorithm

Parameters	Lead	Nitrite
R^2	0.95	0.96
Mean absolute error (MAE)	4.3 ppm	5.25 ppm
Root mean square error (RMSE)	6.36 ppm	6.73 ppm
Cross-validated R^2	0.87 ± 0.082	0.945 ± 0.023

results due to overfitting of data and high amount of variance. Therefore, the features provided to this particular model were the green colour intensity from RGB colour model and saturation from HSV colour model of each image, since these two features showed the best trend with concentration of analyte, as shown in SI, Fig. S2(a–d). The selected features are justified by the strong absorption of the pink chromophores in the green region of the visible spectrum (Fig. 4(a and b)) and by the fact that the saturation parameter is minimally affected by variations in illumination.

An actual *vs.* predicted plot was developed for the trained model with both analytes. The predicted points are seen to cluster along the diagonal regression line, as seen in Fig. 6(f and g), indicating that this model is a reliable predictor. Further analysis of mean absolute error and root mean square error was performed using the equations below and the results are given in Table 1.

Where, P signifies the number of data points in sample

$$\mathrm{MAE} = \frac{1}{P}\sum_{j=1}^{P}\left|\left(m_j - \hat{m}\right)\right| \quad (1)$$

$$\mathrm{RMSE} = \sqrt{\frac{1}{P}\sum_{j=1}^{P}\left(m_j - \hat{m}\right)^2} \quad (2)$$

m_j = observed values (actual values) and $\hat{m}$ = predicted values (model's predictions).

The regression was stored in pickle files that can be integrated with the Tkinter module in Python to design a user-friendly desktop application. The output from the desktop application developed for this program was given in terms of three categories, which were low strength (<10 ppm), moderate strength (10–50 ppm) and high strength (>50 ppm) loads of contamination. Low strength contamination is meant to indicate low pollutant load that has to be processed for effluent treatment. The second category, *i.e.* moderate load is indicative of a requirement for secondary treatments such as chemical precipitation or bio-adsorption for enhanced treatment of effluent. Lastly, the high-strength load suggests the requirement of intensive multi-step removal processes to comply with wastewater treatment standards. The false positive and false negative rate was calculated for the prediction algorithm at the LOD in a decision matrix that is given in Table S4. The algorithm is seen to provide a false positive of 10% while the false negative rate is of 25% for Pb^{2+}. In case of NO_2^-, the false positive and negative rates are 0% and 15%, respectively. These results show strong specificity for both analytes near the screening threshold. To further boost the robustness of prediction, the GUI displays a 'Error/Please try again' message when the pink colour is indistinguishable, to reduce cases of false-positive prediction near the detection limit.

Spiked water sample analysis

To test the accuracy of the sensors on real samples, recovery studies were performed on spiked water collected from 5 different regions. 2 samples were collected from various locations along the bank of the Ganges river, 1 sample were collected from a pond in IIT Kharagpur, and 2 samples were collected from agricultural run-off water sources in Salua area, Kharagpur. The samples were spiked with known concentrations of both analytes and measured thrice by gold standard methods and developed paper sensor from this study. Gold standards used for analysis of spiked samples for lead was Atomic Absorption Spectroscopy and for nitrite was UV-visible spectroscopy. The accuracy was calculated using the following formula:

$$\text{Average accuracy } \% = \frac{\text{Predicted concentration}}{\text{Actual concentration}} \times 100$$

The trained model demonstrated excellent accuracy, which was 100.6% for lead samples and 102% for nitrite samples. The results discussed in Table 2, proves the excellent practical application of this prediction model.

Real-world wastewater often exhibits turbidity or inherent coloration due to suspended solids, dissolved organic matter, corrosion products, and residual industrial dyes, which can influence optical measurements in colorimetric sensing. In

Table 2 Prediction of unknown lead and nitrite concentration in spiked samples

Samples	Actual concentration (ppm)	Predicted concentration (ppm)	Accuracy percentage (%)	Average accuracy (%) ± standard deviation
Lead				
S1	32.7	32.2	98.4	100.6 ± 3.9
S2	84.9	87.5	103.06	
S3	96.4	98.75	102.43	
S4	51.3	49.16	104.3	
S5	42.56	40.33	94.7	
Nitrite				
S1	40.6	38.2	94.1	101.86 ± 6.13
S2	62.7	63.5	101.2	
S3	11.5	12.7	110.4	
S4	28.7	30.07	104.7	
S5	83.8	82.9	98.9	

Table 3 Comparison of the current study with similar literature

Type of testing kit	Principle and method	Multiplexed	Detection range	Assay time	Field-ready?	Cost of paper sensor	Reference
Lead test strips, colorimetric	Uses rhodizonic acid to detect lead by colour change on a strip, quantified through visual scale comparison	No	20–500 ppm	10 min	Yes	~$10	Merck product datasheet
Colorimetric and paper-based detection of lead	Uses AgNP/PVA nanoparticle aggregation as a colorimetric indicator for lead, though reliant on lab-synthesized particles with limited stability	No	0.1–1 ppm	15 minutes	Experimental	~$0.20	*Microchemical Journal* (2019)[68]
Paper-based and colorimetric dual-mode detection of arsenic(III) and lead(II)	Uses AuNP/glucose nanoparticles as indicators, requiring synthesis of modified gold nanoparticles stored in suspension	Yes	0.2–1 ppm	5 minutes	Experimental	~$1	*RSC Advances* (2021)[69]
Eco-friendly paper-based colorimetric sensor for portable and rapid detection of lead(II) ions	Uses eriochrome black T and bromothymol blue on dye-soaked paper strips to detect lead *via* colour change	No	60–140 ppm	~5 minutes	No	~$0.1	Springer Nature Link (2025)[70]
Paper-based microfluidic devices for the analysis of nitrite and glucose	Patterned adhesive tape on filter paper with Griess and TMB enabled multiplexed colorimetric detection, quantified by linear regression	Yes	3 ppm for nitrite	10 min	Experimental	<$0.50	*Sensors* (2019)[71]
Origami colorimetric paper-based sensor for analysis of nitrite	Uses an origami structure to separate Griess reagent components for stability, enabling single-analyte detection	No	0.27 ppm	15 min	Yes	<$0.50	*Sensors and Diagnostics* (2025)[61]
Paper-based microfluidic colorimetric sensor on a 3D printed support	Uses Griess reagent-soaked paper discs mounted on a 3D support for colorimetric readout	No	0.12 ppm	15 min	Experimental	<$1	*Environmental Research* (2022)[72]
Colorimetric multiplexed paper sensor with smartphone and ML integration for lead and nitrite sensing	Paper-based platform with sodium rhodizonate and Griess reagents enabled synthesis-free dual detection, with colour changes quantified by a machine learning desktop app., providing rapid and reliable analysis	Yes	3 ppm for nitrite 7 ppm for lead	5 min	Yes	<$0.50	Present study

practical use, the paper substrate can partially mitigate physical interferences such as turbidity by retaining larger particulates during capillary wicking, allowing the colorimetric reaction to occur within the paper matrix. The wicking and drying processes further help localize the chromophore formation within the porous substrate, reducing the influence of suspended solids. Image analysis is performed on a defined region of interest using fixed acquisition conditions of the camera. Nevertheless, highly turbid or strongly coloured samples may still influence the optical readout, representing a known limitation of paper-based colorimetric screening systems. On paper substrates, droplet spreading and evaporation-driven effects, such as coffee-ring formation, may further contribute to signal variability. In the present system, capillary wicking within the paper matrix and the incorporation of chitosan promote more uniform reagent distribution and help reduce coffee-ring effects commonly observed in paper-based Griess reactions (Fig. S4). In addition, smartphone-based image-dependent colorimetric readouts are inherently sensitive to variations in sample appearance and lighting conditions. Highly turbid or strongly coloured samples may also impact the accuracy of the optical response, representing a practical limitation of paper-based screening platforms and highlighting the need for future improvements through surface engineering or advanced image-processing strategies. Recent investigations have shown that advanced materials and surface-engineering methods can improve optical detection in complex wastewater matrices. Strain-responsive photothermal super-wetting systems and elastic graphene-modified sponges have shown enhanced fluid dynamics and separation in oily emulsions and viscous multi-component wastewater under practical conditions.[64] Biomimetic Yin–Yang membranes with dual super-wettabilities demonstrate that controlled wettability and surface design may effectively separate complex tri-phase oil–water mixtures, which can effectively address challenges associated with complex wastewater matrices.[65] Further, mosaic-patterned functional surfaces that hold droplet arrays illustrate how precise control over droplet spreading and evaporation may make optical readout more stable and consistent in screening and environmental monitoring applications.[66] Further, the use of machine learning for interpreting image-based colorimetric signals are being increasingly employed in recent research to extract meaningful information from complex chemical data, when signals are influenced by multiple interacting factors such as sample heterogeneity and measurement conditions.[67] These trends in research for pre-processing samples and post-processing datasets can help in further strengthening the application of paper-based screening tools as presented in our study.

Comparison with existing technology

The existing technology in the field of lead and nitrite ion sensing has demonstrated varying levels of sensitivity and field applicability. However, most existing studies focus on isolated detection of one ion and qualitative analysis of the ions using visual colour readout. Furthermore, many of the technologies developed have utilized synthesis methods to incorporate nanomaterials into paper, which limits its reproducibility, stability and ease of fabrication. This study aims to bridge this gap between cost of fabrication, sensitivity and ease of operation by using a dry phase reagent deposited sensing strategy along with semi-quantitative categorical readout.

In summary, as seen in Table 3, many paper-based colorimetric platforms have achieved better detection limits for either lead or nitrite through nanoparticle incorporation, or by exploiting paper's innate properties for different designs. However, these devices can be seen to involve multi-step reagent preparation and limited field-employability. The multiplexed sensor presented in this study addresses these constraints by offering simultaneous detection of both analytes at modest detection limits, coupled with a dry-state reagent pellet design that enhances stability and handling. The primary expenses for this sensor were the acquisition of a smartphone, a laptop, and an image capture dark box apparatus, amounting to less than $300. Assuming consumers own a smartphone and a personal laptop, the fixed expenditures may be reduced to about $50. The chemicals and the pellet incur a recurrent cost of roughly $5, sufficient for over 300 paper devices. Each paper device amounts to less than $0.50 for fabrication costs, a further breakdown of which is given in Table S2. This cost efficiency further supports the robustness of this prototype lead and nitrite detection kit. This pen-and-paper microfluidic platform therefore combines simplicity, low cost, and real-world applicability, making it well-suited for deployment in environmental pollution screening kits.

Conclusions

The present study successfully demonstrates the development of a low-cost, field-deployable colorimetric screening tool capable of simultaneously quantifying lead and nitrite in polluted water without requiring complex pre- or post-treatment steps. Its user-friendly fabrication and reagent pencil innovation ensure reagent stability and ease of transport, making it suitable for preliminary water testing at remote locations. Moreover, the reagent pencil strategy for reagent stabilisation can be extended to other colorimetric reagents that typically suffer from limited shelf-life in paper-based assays. The device's dual-zone architecture effectively prevents signal interference, while its robustness against ambient temperature (0–40 °C) and humidity variations (30–99%) addresses practical challenges in diverse climatic conditions. Integration with smartphone-based colorimetric analysis and machine learning enhances the precision and accessibility of analyte concentration predictions, further supported by a graphical user interface for ease of use. Validation with spiked environmental samples confirms high accuracy and reliability within the ppm concentration range. The limit of detection of 3 ppm for nitrites and the LOD of 7 ppm for lead lies within the range of acceptable limits of lead in untreated effluents from various industrial activities. The prediction errors of 6 ppm are reflective of the colorimetric paper-based sensor's intrinsic variability and the ppm scale screening application of these devices. The use of

5-fold cross-validation was employed to reduce overfitting and to provide a realistic estimate of model performance within a laboratory limited dataset. Expansion of the training dataset to include a wider range of concentrations, matrix compositions, and real wastewater samples is expected to further improve model generalization and represents an important direction for enhancement of this paper-based tool. While precise quantification near the detection limit remains challenging, the proposed device is well suited for semi-quantitative assessment of contamination levels relevant to industrial wastewater monitoring. Accordingly, the sensor is designed for primary screening and categorical classification of samples into low, moderate, and high contamination levels rather than precise quantification. Such a screening-oriented approach enables rapid decision-making and can be particularly valuable for long-term urban and rural water quality monitoring strategies. Future work in this direction can focus on extending detection limits to the ppb level, potentially through hybridizing this colorimetric approach with complementary analytical methods such as electrochemical or fluorescence sensors. Overall, this research lays a strong foundation for affordable and portable water quality screening tools that can empower widespread environmental and public health surveillance.

Author contributions

Akashlina Basu – conceptualisation, investigation, formal analysis, writing – original draft. Pooja C. Asani – writing – original draft. Kalpita Nath – investigation (AAS experiments). Soumen Das – conceptualisation, funding acquisition, supervision and writing – review and editing.

Conflicts of interest

The authors declare that they have no known competing financial interests or personal relationships that could have appeared to influence the work reported in this paper.

Data availability

The authors confirm that all data supporting the findings of this study are available within the article and its supplementary information (SI). Additional supporting data are available from the corresponding author upon request. Supplementary information: details of the machine learning workflow and implementation, including pseudo-code, model evaluation, and a decision matrix; tables on cost analysis and comparative model performance, along with figures illustrating fabrication methods, feature selection, regression analysis, and colour development, and details of minimal reproducible materials. See DOI: https://doi.org/10.1039/d5ra09526c.

Acknowledgements

The authors gratefully acknowledge the Ministry of Education (formerly MHRD), Government of India, for providing financial support. The authors extend their sincere appreciation toward Central Research Facility, IIT Kharagpur, for providing SEM facility. The authors would also like to thank Dr Abhijit Lincon and Mr Rohan Koche for their help in developing the Python algorithm.

References

1 W. Chu, Y. Zhang, D. Li, C. J. Barrow, H. Wang and W. Yang, A Biomimetic Sensor for the Detection of Lead in Water, *Biosens. Bioelectron.*, 2015, **67**, 621–624, DOI: 10.1016/J.BIOS.2014.09.077.

2 S. Mitra, A. J. Chakraborty, A. M. Tareq, T. B. Emran, F. Nainu, A. Khusro, A. M. Idris, M. U. Khandaker, H. Osman, F. A. Alhumaydhi and J. Simal-Gandara, Impact of Heavy Metals on the Environment and Human Health: Novel Therapeutic Insights to Counter the Toxicity, *J. King Saud Univ., Sci.*, 2022, **34**(3), 101865, DOI: 10.1016/j.jksus.2022.101865.

3 H. Nguyen, Y. Sung, K. O'Shaughnessy, X. Shan and W. C. Shih, Smartphone Nanocolorimetry for On-Demand Lead Detection and Quantitation in Drinking Water, *Anal. Chem.*, 2018, **90**(19), 11517–11522, DOI: 10.1021/ACS.ANALCHEM.8B02808/ASSET/IMAGES/LARGE/AC-2018-02808M_0008.JPEG.

4 J. Kasten-Jolly, Y. Heo and D. A. Lawrence, Impact of Developmental Lead Exposure on Splenic Factors, *Toxicol. Appl. Pharmacol.*, 2010, **247**(2), 105–115, DOI: 10.1016/j.taap.2010.06.003.

5 P. Pathak, J. H. Hwang, R. H. T. Li, K. L. Rodriguez, M. M. Rex, W. H. Lee and H. J. Cho, Flexible Copper-Biopolymer Nanocomposite Sensors for Trace Level Lead Detection in Water, *Sens. Actuators, B*, 2021, **344**, 130263, DOI: 10.1016/J.SNB.2021.130263.

6 H. Singh, A. Bamrah, S. K. Bhardwaj, A. Deep, M. Khatri, K. H. Kim and N. Bhardwaj, Nanomaterial-Based Fluorescent Sensors for the Detection of Lead Ions, *J. Hazard. Mater.*, 2021, **407**, 124379, DOI: 10.1016/J.JHAZMAT.2020.124379.

7 K. Shrivas, B. Sahu, M. K. Deb, S. S. Thakur, S. Sahu, R. Kurrey, T. Kant, T. K. Patle and R. Jangde, Colorimetric and Paper-Based Detection of Lead Using PVA Capped Silver Nanoparticles: Experimental and Theoretical Approach, *Microchem. J.*, 2019, **150**, 104156, DOI: 10.1016/J.MICROC.2019.104156.

8 H. Na Kim, W. Xiu Ren, J. Seung Kim and J. Yoon, Fluorescent and Colorimetric Sensors for Detection of Lead, Cadmium, and Mercury Ions, *Chem. Soc. Rev.*, 2012, **41**(8), 3210–3244, DOI: 10.1039/c1cs15245a.

9 G. A. C. Madlangbayan, K. G. N. Quiton and M. C. Lu, Removal of Lead and Nitrate from Simulated Lead- and Nitrate-Containing Wastewater via Hydroxide Precipitation, *Processes*, 2024, **12**(8), 1662, DOI: 10.3390/PR12081662.

10 T. E. Aniyikaiye, T. Oluseyi, J. O. Odiyo and J. N. Edokpayi, Physico-Chemical Analysis of Wastewater Discharge from Selected Paint Industries in Lagos, Nigeria, *Int. J. Environ. Res. Public Health*, 2019, **16**(7), 1235, DOI: 10.3390/ijerph16071235.

11 M. M. Abbas, K. S. Husien and I. G. Zainal, Assessment of Lead and Cadmium in Some Industrial Wastewater in Kirkuk City, *J. Pioneering Med. Sci.*, 2024, **13**(1), 1–5, DOI: 10.61091/jpms202413101.

12 N. Muhammad, M. Nafees, L. Ge, M. H. Khan, M. Bilal, W. P. Chan and G. Lisak, Assessment of Industrial Wastewater for Potentially Toxic Elements, Human Health (Dermal) Risks, and Pollution Sources: A Case Study of Gadoon Amazai Industrial Estate, Swabi, Pakistan, *J. Hazard. Mater.*, 2021, **419**, 126450, DOI: 10.1016/J.JHAZMAT.2021.126450.

13 S. Patel, R. Jamunkar, D. Sinha, Monisha, T. K. Patle, T. Kant, K. Dewangan and K. Shrivas, Recent Development in Nanomaterials Fabricated Paper-Based Colorimetric and Fluorescent Sensors: A Review, *Trends Environ. Anal. Chem.*, 2021, **31**, e00136, DOI: 10.1016/j.teac.2021.e00136.

14 A. Das, K. Krishna, R. Kumar, A. Das, S. Sengupta and J. G. Ghosh, Tracing Lead Contamination in Foods in the City of Kolkata, India, *Environ. Sci. Pollut. Res.*, 2016, **23**(22), 22454–22466, DOI: 10.1007/S11356-016-7409-3/FIGURES/8.

15 S. Chakraborty, P. Chakraborty and B. N. Nath, Lead Distribution in Coastal and Estuarine Sediments around India, *Mar. Pollut. Bull.*, 2015, **97**(1–2), 36–46, DOI: 10.1016/J.MARPOLBUL.2015.05.056.

16 J. Nam, I. B. Jung, B. Kim, S. M. Lee, S. E. Kim, K. N. Lee and D. S. Shin, A Colorimetric Hydrogel Biosensor for Rapid Detection of Nitrite Ions, *Sens. Actuators, B*, 2018, **270**, 112–118, DOI: 10.1016/J.SNB.2018.04.171.

17 M. Arvand, N. Arjmandi, M. Shakibaie, S. Jafarinejad, R. Shahghadami and P. Sasanpour, Colorimetric Microfluidic Paper-Based Sensor for Determination of Nitrite in Drinking Water with Enhanced Color Development, *J. Phys. D: Appl. Phys.*, 2020, **53**(35), 355403, DOI: 10.1088/1361-6463/AB8E7A.

18 G. Li, Y. Xia, Y. Tian, Y. Wu, J. Liu, Q. He and D. Chen, Review—Recent Developments on Graphene-Based Electrochemical Sensors toward Nitrite, *J. Electrochem. Soc.*, 2019, **166**(12), B881–B895, DOI: 10.1149/2.0171912JES/XML.

19 Y. Zhang, N. Love and M. Edwards, Nitrification in Drinking Water Systems, *Crit. Rev. Environ. Sci. Technol.*, 2009, **39**(3), 153–208, DOI: 10.1080/10643380701631739.

20 K. G. Lopez, J. Xiao, C. Crockett, C. Lytle, H. Grubbs and M. Edwards, Seasonal Fluctuations in Nitrate Levels Can Trigger Lead Solder Corrosion Problems in Drinking Water, *Environ. Sci. Technol. Lett.*, 2023, **10**(1), 21–26, DOI: 10.1021/ACS.ESTLETT.2C00581/ASSET/IMAGES/LARGE/EZ2C00581_0003.JPEG.

21 H. Wu, X. Shen, D. Huo, Y. Ma, M. Bian, C. Shen and C. Hou, Fluorescent and Colorimetric Dual-Readout Sensor Based on Griess Assay for Nitrite Detection, *Spectrochim. Acta, Part A*, 2020, **225**, 117470, DOI: 10.1016/J.SAA.2019.117470.

22 Y. H. Zhan, R. Sun, W. J. Zhu, Y. J. Xu and J. F. Ge, An Oxazine-Based near-Infrared Fluorescent Probe for Selective in Cellular Imaging of Exogenous Nitrite, *Sens. Actuators, B*, 2017, **240**, 1283–1290, DOI: 10.1016/J.SNB.2016.09.113.

23 M. M. H. Al-Gayyar, H. M. Hassan, A. Alyoussef, A. Abbas, M. M. Darweish and A. A. El-Hawwary, Nigella Sativa Oil Attenuates Chronic Nephrotoxicity Induced by Oral Sodium Nitrite: Effects on Tissue Fibrosis and Apoptosis, *Redox Rep.*, 2016, **21**(2), 50, DOI: 10.1179/1351000215Y.0000000035.

24 K. Karar, A. K. Gupta, A. Kumar and A. K. Biswas, Characterization and Identification of the Sources of Chromium, Zinc, Lead, Cadmium, Nickel, Manganese and Iron in PM10 Particulates at the Two Sites of Kolkata, India, *Environ. Monit. Assess.*, 2006, **120**(1–3), 347–360, DOI: 10.1007/s10661-005-9067-7.

25 L. Patro and S. Mishra, Evaluation Of Nitrate And Nitrite Contents In Water Of Chilika Lagoon, Odisha, India, *International Journal of Advance Research and Innovative Ideas in Education*, 2015, **1**(5), 979–985.

26 S. Narayan Sinha, N. Desai, G. Patel, M. Mansuri and V. Shivgotra, Concentration of Nitrite in Respirable Particulate Matter of Ambient Air in Vadodara, Gujarat, India, *J. Environ. Biol.*, 2010, **31**(3), 375–378.

27 A. Verma, A. Kumar Rawat and N. More, Extent of Nitrate and Nitrite Pollution in Ground Water of Rural Areas of Lucknow, U.P., India, *Curr. World Environ.*, 2014, **9**(1), 114–122, DOI: 10.12944/CWE.9.1.17.

28 Central Pollution Control Board, https://www.cpcb.nic.in/.

29 Pure Earth, *India's Lead Crisis: A Call to Action*, Pure Earth, New York, 2022.

30 Council of Scientific & Industrial Research (CSIR) and NITI Aayog, *Assessment of Lead Impact on Human Health in India and India's Response*, Government of India, 2022.

31 Q. Z. Zhai, J. M. Li and J. P. Zhang, Spectrophotometric Determination of Lead in Tea Leaf Sample with Dibromo-p-Chloro-Arsenazo, *Asian J. Chem.*, 2013, **25**(1), 538–540, DOI: 10.14233/AJCHEM.2013.13577.

32 K. Shrivas and D. K. Patel, Separation and Preconcentration of Trace Level of Lead in One Drop of Blood Sample by Using Graphite Furnace Atomic Absorption Spectrometry, *J. Hazard. Mater.*, 2010, **176**(1–3), 414–417, DOI: 10.1016/J.JHAZMAT.2009.11.045.

33 A. Schütz, I. A. Bergdahl, A. Ekholm and S. Skerfving, Measurement by ICP-MS of Lead in Plasma and Whole Blood of Lead Workers and Controls, *Occup. Environ. Med.*, 1996, **53**(11), 736–740, DOI: 10.1136/OEM.53.11.736.

34 A. C. Todd and P. J. Landrigan, X-Ray Fluorescence Analysis of Lead in Bone, *Environ. Health Perspect.*, 1993, **101**(6), 494–495, DOI: 10.1289/EHP.93101494.

35 T. Zerihun and P. Gründler, Electrically Heated Cylindrical Microelectrodes. Determination of Lead on Pt by Cyclic Voltammetry and Cathodic Stripping Analysis, *J. Electroanal. Chem.*, 1996, **415**(1–2), 85–88, DOI: 10.1016/S0022-0728(96)04711-0.

36 S. Chamandust, M. R. Mehrasebi, K. Kamali, R. Solgi, J. Taran, F. Nazari and M. J. Hosseini, Simultaneous Determination of Nitrite and Nitrate in Milk Samples by Ion Chromatography Method and Estimation of Dietary Intake, *Int. J. Food Prop.*, 2016, **19**(9), 1983–1993, DOI: 10.1080/10942912.2015.1091007.

37 Y. Shen, Q. Zhang, X. Qian and Y. Yang, Practical Assay for Nitrite and Nitrosothiol as an Alternative to the Griess Assay or the 2,3-Diaminonaphthalene Assay, *Anal. Chem.*, 2015, **87**(2), 1274–1280, DOI: 10.1021/AC5039779.

38 J. Chen, S. Pang, L. He and S. R. Nugen, Highly Sensitive and Selective Detection of Nitrite Ions Using Fe3O4@SiO2/Au Magnetic Nanoparticles by Surface-Enhanced Raman Spectroscopy, *Biosens. Bioelectron.*, 2016, **85**, 726–733, DOI: 10.1016/J.BIOS.2016.05.068.

39 Z. Kalaycıoğlu and F. B. Erim, Simultaneous Determination of Nitrate and Nitrite in Fish Products with Improved Sensitivity by Sample Stacking-Capillary Electrophoresis, *Food Anal. Methods*, 2016, **9**(3), 706–711, DOI: 10.1007/S12161-015-0241-4.

40 T. Cherian and B. Narayana, A New System for the Spectrophotometric Determination of Trace Amounts of Nitrite in Environmental Samples, *J. Braz. Chem. Soc.*, 2006, **17**(3), 577–581, DOI: 10.1590/S0103-50532006000300022.

41 J. Wu, X. Wang, Y. Lin, Y. Zheng and J. M. Lin, Peroxynitrous-Acid-Induced Chemiluminescence Detection of Nitrite Based on Microfluidic Chip, *Talanta*, 2016, **154**, 73–79, DOI: 10.1016/J.TALANTA.2016.03.062.

42 J. Davis, M. J. Moorcroft, S. J. Wilkins, R. G. Compton and M. F. Cardosi, Electrochemical Detection of Nitrate and Nitrite at a Copper Modified Electrode, *Analyst*, 2000, **125**(4), 737–742, DOI: 10.1039/A909762G.

43 Y. T. Tai, C. Y. Cheng, Y. S. Chen and F. H. Ko, A Hydrogel-Based Chemosensor Applied in Conjunction with a Griess Assay for Real-Time Colorimetric Detection of Nitrite in the Environment, *Sens. Actuators, B*, 2022, **369**, 132298, DOI: 10.1016/J.SNB.2022.132298.

44 F. Li, Y. Hu, Z. Li, J. Liu, L. Guo and J. He, Three-Dimensional Microfluidic Paper-Based Device for Multiplexed Colorimetric Detection of Six Metal Ions Combined with Use of a Smartphone, *Anal. Bioanal. Chem.*, 2019, **411**(24), 6497–6508, DOI: 10.1007/S00216-019-02032-5/TABLES/2.

45 A. K. Ellerbee, S. T. Phillips, A. C. Siegel, K. A. Mirica, A. W. Martinez, P. Striehl, N. Jain, M. Prentiss and G. M. Whitesides, Quantifying Colorimetric Assays in Paper-Based Microfluidic Devices by Measuring the Transmission of Light through Paper, *Anal. Chem.*, 2009, **81**(20), 8447–8452, DOI: 10.1021/AC901307Q/SUPPL_FILE/AC901307Q_SI_001.PDF.

46 A. W. Martinez, S. T. Phillips, M. J. Butte and G. M. Whitesides, Patterned Paper as a Platform for Inexpensive, Low-Volume, Portable Bioassays, *Angew Chem. Int. Ed. Engl.*, 2007, **46**(8), 1318–1320, DOI: 10.1002/ANIE.200603817.

47 O. S. P. Kare, D. Das, K. Chaudhury and S. Das, Hand-Drawn Electrode Based Disposable Paper Chip for Artificial Sweat Analysis Using Impedance Spectroscopy, *Biomed. Microdevices*, 2021, **23**(4), 1–12, DOI: 10.1007/S10544-021-00578-9/TABLES/3.

48 A. Charbaji, H. Heidari-Bafroui, C. Anagnostopoulos and M. Faghri, A New Paper-Based Microfluidic Device for Improved Detection of Nitrate in Water, *Sensors*, 2021, **21**(1), 102, DOI: 10.3390/S21010102.

49 S. Sinha, A. Basu, J. Shukla, S. Dasgupta, G. Dutta and S. Das, A Smartphone-Integrated Low-Cost, Reagent-Free, Non-Destructive Dried Blood Spot-Based Paper Sensor for Hematocrit Measurement, *Anal. Methods*, 2023, **15**(29), 3532–3542, DOI: 10.1039/D3AY00688C.

50 S. Biswas, A. Pal, K. Chaudhury and S. Das, Polyaniline Functionalized Impedimetric Paper Sensor for Urine PH Measurement, *IEEE Sens. J.*, 2021, **21**(13), 14474–14482, DOI: 10.1109/JSEN.2020.3013405.

51 A. Nilghaz, L. Guan, W. Tan and W. Shen, Advances of Paper-Based Microfluidics for Diagnostics - The Original Motivation and Current Status, *ACS Sens.*, 2016, **1**(12), 1382–1393, DOI: 10.1021/ACSSENSORS.6B00578/ASSET/IMAGES/LARGE/SE-2016-00578P_0004.JPEG.

52 E. Carrilho, A. W. Martinez and G. M. Whitesides, Understanding Wax Printing: A Simple Micropatterning Process for Paper-Based Microfluidics, *Anal. Chem.*, 2009, **81**(16), 7091–7095, DOI: 10.1021/ac901071p.

53 O. K. Siva Prakasam, A. Basu, K. Chaudhury and S. Das, On Paper Characterisation of Droplet and Evaporation Study Using Impedance Spectroscopy, *Anal. Methods*, 2024, **16**(16), 2533–2542, DOI: 10.1039/d4ay00303a.

54 N. Anjali, S. Das and S. Chakraborty, Simultaneous Quantitative Detection of Hematocrit and Hemoglobin from Whole Blood Using a Multiplexed Paper Sensor with a Smartphone Interface, *Lab Chip*, 2023, **23**(2), 318–329, DOI: 10.1039/D2LC00456A.

55 Z. Chen, Z. Zhang, J. Qi, J. You, J. Ma and L. Chen, Colorimetric Detection of Heavy Metal Ions with Various Chromogenic Materials: Strategies and Applications, *J. Hazard. Mater.*, 2023, **441**, 129889, DOI: 10.1016/J.JHAZMAT.2022.129889.

56 N. Uhlikova, M. I. G. S. Almeida, I. D. McKelvie and S. D. Kolev, Microfluidic Paper-Based Analytical Device for the Speciation of Inorganic Nitrogen Species, *Talanta*, 2024, **271**, 125671, DOI: 10.1016/J.TALANTA.2024.125671.

57 A. Shahvar, D. Shamsaei and M. Saraji, A Portable Smartphone-Based Colorimetric Sensor for Rapid Determination of Water Content in Ethanol, *Measurement*, 2020, **150**, 107068, DOI: 10.1016/J.MEASUREMENT.2019.107068.

58 H. T. Mitchell, I. C. Noxon, C. A. Chaplan, S. J. Carlton, C. H. Liu, K. A. Ganaja, N. W. Martinez, C. E. Immoos, P. J. Costanzo and A. W. Martinez, Reagent Pencils: A New Technique for Solvent-Free Deposition of Reagents onto Paper-Based Microfluidic Devices, *Lab Chip*, 2015, **15**(10), 2213–2220, DOI: 10.1039/c5lc00297d.

59 C. H. Liu, I. C. Noxon, L. E. Cuellar, A. L. Thraen, C. E. Immoos, A. W. Martinez and P. J. Costanzo, Characterization of Reagent Pencils for Deposition of Reagents onto Paper-Based Microfluidic Devices, *Micromachines*, 2017, **8**(8), 242, DOI: 10.3390/mi8080242.

60 P. A. Bizirtsakis, M. Tarara, A. Tsiasioti, P. D. Tzanavaras and G. Z. Tsogas, Development of a Paper-Based Analytical Method for the Selective Colorimetric Determination of

Bismuth in Water Samples, *Chemosensors*, 2022, **10**(7), 265, DOI: 10.3390/chemosensors10070265.

61 D. Gregucci, M. M. Calabretta, F. Nazir, R. J. R. Arias, F. Biondi, R. Desiderio and E. Michelini, An Origami Colorimetric Paper-Based Sensor for Sustainable on-Site and Instrument-Free Analysis of Nitrite, *Sens. Diagn.*, 2025, **4**(3), 239–246, DOI: 10.1039/d4sd00308j.

62 M. N. Abbas and G. A. Mostafa, Determination of Traces of Nitrite and Nitrate in Water by Solid Phase Spectrophotometry, *Anal. Chim. Acta*, 2000, **410**(1–2), 185–192, DOI: 10.1016/S0003-2670(00)00736-4.

63 J. Xu, X. Xu and W. Verstraete, Adaptation of E. Coli Cell Method for Micro-Scale Nitrate Measurement with the Griess Reaction in Culture Media, *J. Microbiol. Methods*, 2000, **41**(1), 23–33, DOI: 10.1016/S0167-7012(00)00141-X.

64 L. Jiao, Z. Pan, D. Li, Y. Hu, Q. Guo, M. Wang, C. Ding, X. Luo, K. Deng, G. Yang, L. Jiao, Z. Pan, Y. Hu, Q. Guo, X. Luo, K. Deng, G. Yang, M. Wang, C. Ding and D. Li, Elastic-Photothermal Graphene-Modified Super-Wetting Sponge for Efficient Purification of Multicomponent Oil-Water Emulsions, *Adv. Funct. Mater.*, 2026, **36**(4), e12912, DOI: 10.1002/ADFM.202512912.

65 L. Jiao, Y. Huang, Y. Hu, Y. Yang, H. Chen, N. Zhou, Q. Guo, H. Wu, A. Xia, X. Zhao, G. Hu and R. Chen, Yin-Yang Membrane with Dual Superwettabilities for Controllable Separation of Complex Oil/Water Mixtures, *Sep. Purif. Technol.*, 2024, **338**, 126513, DOI: 10.1016/J.SEPPUR.2024.126513.

66 L. Jiao, Y. Wu, Y. Hu, Q. Guo, H. Wu, H. Yu, L. Deng, D. Li and L. Li, Mosaic Patterned Surfaces toward Generating Hardly-Volatile Capsular Droplet Arrays for High-Precision Droplet-Based Storage and Detection, *Small*, 2023, **19**(14), 2206274, DOI: 10.1002/SMLL.202206274.

67 R. Houhou and T. Bocklitz, Trends in Artificial Intelligence, Machine Learning, and Chemometrics Applied to Chemical Data, *Anal. Sci. Adv.*, 2021, **2**(3–4), 128–141, DOI: 10.1002/ANSA.202000162.

68 K. Shrivas, B. Sahu, M. K. Deb, S. S. Thakur, S. Sahu, R. Kurrey, T. Kant, T. K. Patle and R. Jangde, Colorimetric and Paper-Based Detection of Lead Using PVA Capped Silver Nanoparticles: Experimental and Theoretical Approach, *Microchem. J.*, 2019, **150**, 104156, DOI: 10.1016/J.MICROC.2019.104156.

69 B. Sahu, R. Kurrey, M. K. Deb, K. Shrivas, I. Karbhal and B. R. Khalkho, A Simple and Cost-Effective Paper-Based and Colorimetric Dual-Mode Detection of Arsenic(Iii) and Lead(Ii) Based on Glucose-Functionalized Gold Nanoparticles, *RSC Adv.*, 2021, **11**(34), 20769–20780, DOI: 10.1039/d1ra02929k.

70 N. M. Poovadichalil, A. Ullah, M. R. Maurya, A. Hasan and K. K. Sadasivuni, Eco-Friendly Paper-Based Colorimetric Sensor for Portable and Rapid Detection of Lead (II) Ions in Aqueous Environment, *Int. J. Environ. Sci. Technol.*, 2025, **22**, 15467–15478, DOI: 10.1007/s13762-025-06636-6.

71 P. Yu, M. Deng and Y. Yang, New Single-Layered Paper-Based Microfluidic Devices for the Analysis of Nitrite and Glucose Built via Deposition of Adhesive Tape, *Sensors*, 2019, **19**(19), 4082, DOI: 10.3390/s19194082.

72 P. Rajasulochana, Y. Ganesan, P. S. Kumar, S. Mahalaxmi, F. Tasneem, M. Ponnuchamy and A. Kapoor, Paper-Based Microfluidic Colorimetric Sensor on a 3D Printed Support for Quantitative Detection of Nitrite in Aquatic Environments, *Environ. Res.*, 2022, **208**, 112745, DOI: 10.1016/j.envres.2022.112745.